PADDY RICE POROSITY PREDICTION BASED ON SNAKE ALGORITHM OPTIMIZED SUPPORT VECTOR REGRESSION
/
基于蛇算法优化支持向量回归的稻谷孔隙率预测

Zhi-Qi ZHANG[1,2], Lin WAN [*1,2], Gang CHE [*1,2], Hong-Chao WANG[1], Heng PAN[1], Shuo WANG[1]
[1]College of Engineering, Heilongjiang Bayi Agricultural University, Daqing / P.R.China
[2]Key Laboratory of Intelligent Agricultural Machinery Equipment in Heilongjiang Province, Daqing / P.R.China
Tel：+86-459-15245569595; E-mail: 895534729@qq.com
Corresponding author: Lin Wan
DOI: https://doi.org/10.35633/inmateh-76-61

Keywords: *paddy rice, image processing, snake algorithm, support vector regression*

ABSTRACT
During the paddy rice drying process, the uneven spatial distribution of pore spaces within drying chambers poses a significant challenge to accurate porosity characterization and results in inefficient energy utilization. To address this issue, this study proposes a porosity prediction model based on Support Vector Regression (SVR), aimed at effectively monitoring porosity variations during drying and enhancing energy efficiency. Using MATLAB based image processing, the porosity of paddy rice was quantitatively extracted. A Response Surface Methodology (RSM) was then employed to analyze the influence of geometric characteristics, moisture content, and grain bulk height on porosity during drying. To further improve the predictive performance, the SVR model was optimized using the Snake Optimizer (SO) algorithm. The resulting SO-SVR model was evaluated against porosity values derived from image analysis. Experimental results demonstrate that the SO-SVR model achieves high accuracy, with a Root Mean Square Error (RMSE) of 0.0095 and a coefficient of determination (R^2) of 0.9913. Compared to standard SVR and BP neural network models, the proposed model reduces RMSE by 0.0867 and 0.1663, and increases R^2 by 0.0449 and 0.1102, respectively. These findings indicate that the SO-SVR model provides a reliable and efficient approach for predicting paddy rice porosity during drying, offering valuable support for energy-saving and intelligent drying system design.

摘要
针对稻谷干燥过程中，干燥机内稻谷孔隙空间分布不均难以精准解析进而影响稻谷的干燥能耗的问题，建立一种基于支持向量回归（SVR）的稻谷孔隙率预测模型，高效检测稻谷干燥过程中孔隙率的变化，以达到节能效果。本文用 MATLAB 对稻谷图像处理得出稻谷孔隙率，用响应面（RSM）分析稻谷几何参数、含水率、粮堆厚度在稻谷干燥过程中对孔隙率的影响程度，利用蛇算法（SO）对支持向量回归（SVR）模型进行优化，建立稻谷孔隙率预测模型，并与基于图像处理后的稻谷孔隙率进行分析对比。结果表明： SO-SVR 模型的均方根误差（RMSE）为 0.0095、决定系数（R2）为 0.9913，相对于 SVR 和 BP 算法的 RMSE 降低了 0.0867 和 0.1663；R^2 提升了 0.0449 和 0.1102。实验数据表明该模型的预测误差较小，具有更高的准确性，可以有效预测稻谷在干燥过程的孔隙率。

INTRODUCTION
Grain security is a cornerstone of national economic stability and social development. Ensuring food security not only provides a solid foundation for stable economic development but also serves as a key factor in maintaining social stability and strengthening national security (*Fujimori et al., 2019*). According to data from the National Bureau of Statistics, China’s total grain output reached 713 million tons in 2024, marking a 1.6% year-on-year increase, with rice accounting for 29.38% of the total grain production. To ensure rice quality, post-harvest high-moisture rice must undergo drying treatment. Porosity is one of the key parameters for understanding the drying process and energy consumption of rice (*Che et al., 2017*). During the drying process, porosity directly affects ventilation resistance, heat and moisture transfer coefficients, and the adjustment of drying process parameters (*Tong et al., 2023*), thereby influencing energy consumption, drying efficiency, and cost (*Oliveros et al., 2017*). Therefore, accurate detection of paddy rice porosity during drying is of great significance.

However, in practical production operations, there has been a lack of predictive research on paddy rice porosity, particularly in mixed-flow drying systems.

Currently, Moya conducted consolidation tests on paddy rice using a direct measurement method with an oedometer, and based on the experimental data, identified the relationship between porosity and vertical pressure (*Moya et al., 2013*). Martynenko through systematic experimental studies and theoretical analysis, established a relationship between moisture content and porosity, enabling the quantitative characterization of porous media structure parameters (*Martynenko et al., 2008*). Neethirajan employed computed tomography (CT) imaging technology to visualize the granular structures of wheat and pea seeds, calculating the spatial distribution of porosity and other features within the 3D images, including the degree of axial distortion and throat surface area (*Neethirajan et al., 2008*). Khalili proposed a mathematical model describing the relationship between porosity and bulk layer thickness based on experimental data (*Khalili et al., 2014*). Domestic scholars (*Chen et al., 2019)* have demonstrated, through both theoretical analysis and experimental validation, that porosity is influenced by the thickness of the material layer. Tang Fuyuan used an indirect gas displacement method to determine the porosity of paddy rice, analyzing density variations at different depths and establishing a mathematical model for porosity distribution in silo-stored rice (*Tang et al., 2017*). Cheno measured the permeability of two types of sandstone under varying confining pressures and determined their porosity using mercury intrusion porosimeters (MIP). By comparing the 3D geometrical structures of the pore spaces and flow-relevant pore characteristics, the study established a relationship between the differences in permeability and the porosity of the two sandstones (*Cheno et al., 2021*). Additionally, Ge Mengmeng combined the direct measurement method with liquid infiltration techniques to construct a quantitative model of porosity variation under different pressures. Their research further elucidated the relationship between bulk pressure and density, and analyzed the porosity and density distribution characteristics of rice stacks in flat warehouses (*Ge et al., 2021*). Despite significant progress made by researchers at home and abroad in the study of grain porosity, analytical methods currently in use often involve complex procedures and are time-intensive, thereby hindering their applicability and promotion in engineering practice.

In this study, a direct measurement method is employed to calculate paddy rice porosity based on surface images of rice stacks with varying height, using digital image processing techniques. The Design-Expert 13 software is utilized to analyze the influence of geometric parameters, moisture content, and stack height on porosity. Response Surface Methodology is further applied to evaluate and compare the variation in porosity under different influencing factors. A paddy rice porosity prediction model is then developed based on Support Vector Regression optimized by the Snake Algorithm. This model enables prediction of porosity during the rice drying process and provides key parameters for post-harvest drying and storage analysis of rice.

MATERIALS AND METHODS

Materials

The test material was the Songjing No. 16 rice variety, cultivated in Heilongjiang Province. After impurity removal, well-developed and uniformly shaped grains were selected for the experiment. The moisture content of the paddy rice was 2%, and the average grain length, based on measurements from 200 representative kernels, was 9.02 mm.

Mixed-Flow Paddy Drying Rice Experimental Apparatus

This study employed a self-developed bidirectional-ventilation mixed-flow paddy rice drying experimental platform. The overall structure of the mixed-flow dryer is illustrated in Fig. 1. Gravity-fed rice circulation is achieved through a free-flow feeding mechanism. Flow rate control valves are used to adjust the feeding speed, aligning it with the drying intensity to prevent uneven drying caused by excessively fast or slow grain flow. In the dryer, each drying unit comprises a layer of angular inlet ducts and a layer of angular outlet ducts, arranged in a vertically intersecting manner. The angular inlet ducts supply hot air from both sides, forming a mixed-flow drying pattern, while the outlet ducts vent the exhaust air unilaterally. This cross-layer configuration modifies the airflow path of paddy rice during drying, enabling effective balancing of wind pressure, air velocity, and temperature. Such a structural design improves the uniformity of the cyclic drying process.

Fig. 1 - Mixed-flow paddy rice drying experimental device

1. Mixed flow rice dryer; 2. Temperature and humidity sensor; 3. Air inlet pipeline; 4. Grain discharge motor; 5. Unloading device; 6. Control system cabinet; 7. Mixing pipeline; 8. Mixing device; 9. Hot air pipeline; 10. Electric heating control cabinet

The drying section process is shown in Fig. 2. In the drying operation, wet paddy rice is loaded into the dryer through the top inlet and gradually flows downward by gravity until the chamber is filled. The rice sequentially passes through the tempering-drying section, preheating-drying section, mixed-flow drying section, and discharge-drying section, initiating the cyclic drying process. Hot air ducts are connected on both sides of the drying sections. After setting the fan frequency and hot air temperature, heated air is supplied to the system via electric heaters and fans. A hot air mixing unit regulates the air temperature to ensure stable heat supply throughout the drying system.

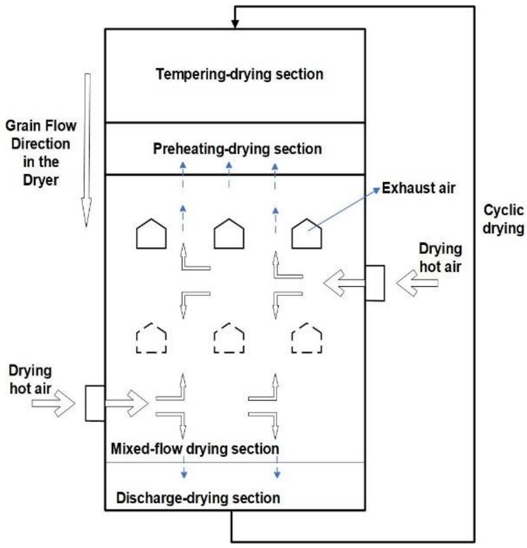

Fig. 2 - Mixed-Flow paddy rice drying process diagram

Additional Measurement Instruments

PM-8188New grain moisture tester; Canon EOS 5D Mark II; micrometer with a precision of 0.01 mm, and a measuring tape.

Data Collection Method

Paddy rice with an initial moisture content of 23.41% was dried to different target moisture levels. A moisture analyzer was used to measure the moisture content of each sample. Individual rice grains were randomly selected, and their lengths (L) were measured using a micrometer with a precision of 0.01 mm. For each group, the average length was calculated based on measurements of 100 intact grains. To simulate the pressure conditions within grain storage silos, incremental loads ranging from 0 to 200 kPa were applied to the rice in the test container. The pressure applied to the grain bulk height was calculated using the hydrostatic pressure equation, as shown in Equation 1, this corresponded to adding 0-12 kg of rice incrementally.

A measuring tape was used to record the resulting grain pile height within the container. In total, 200 groups of data were collected, including measurements of moisture content, grain length, and grain bulk height, for use in subsequent analysis (*Prasad et al., 1973*).

$$P = \rho g h \tag{1}$$

where:

P is the pressure, [Pa];

ρ is the density of paddy rice, [kg/m³];

g is the gravitational acceleration, [m/s²];

h is the grain bulk height, [m]

Porosity Measurement Method

To capture digital images of the grain bulk, a transparent glass test box was employed, featuring an embedded lid made of the same material. The internal dimensions of the box were 300 mm * 200 mm * 400 mm (length * width * height). The shortest dimension of the test container is 200 mm, which is over ten times greater than the average grain length of paddy rice (9.02 mm), thereby fully satisfying the spatial requirements for pressure testing (*Bian et al., 2021*). A Canon digital camera was used for image acquisition. Distortion correction was performed using the MathWorks calibration toolbox. For image segmentation, various thresholding algorithms were compared, and edge-based threshold segmentation was conducted using MATLAB to distinguish the target from the background, the grayscale image and the binarized image were obtained, as illustrated in Fig. 3. Morphological optimization was subsequently applied to the binarized image. Each grain was labeled based on the position of its pixel centroid, and the scaling factor of the imaging system was determined by correlating the pixel area to the actual physical area. Using this factor, the porosity of the paddy rice was calculated. To simulate pressure conditions within a rice silo, different weights of paddy rice were incrementally added to the box, and images were captured after each addition to determine the porosity under varying pressure levels.

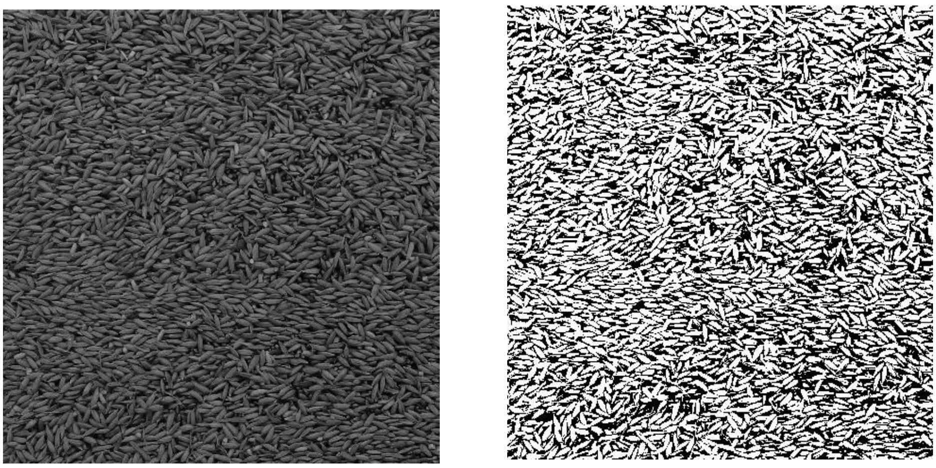

a) The grayscale image *b) The binarized image*

Fig. 3 - The processed images of paddy rice

The porosity formula for paddy rice in their natural piled state is shown in Equation 2. The smaller the difference between the porosity value obtained through image processing and the one from the formula, the higher the accuracy, as illustrated in Fig. 4.

$$\varepsilon = \left(1 - \frac{\rho_b}{\rho_w}\right) \times 100\% \tag{2}$$

where:

ε - the porosity, [%];

ρ_b is the initial density of a paddy rice unit, [kg/m³];

ρ_w - the density of rice particles, [kg/m³]

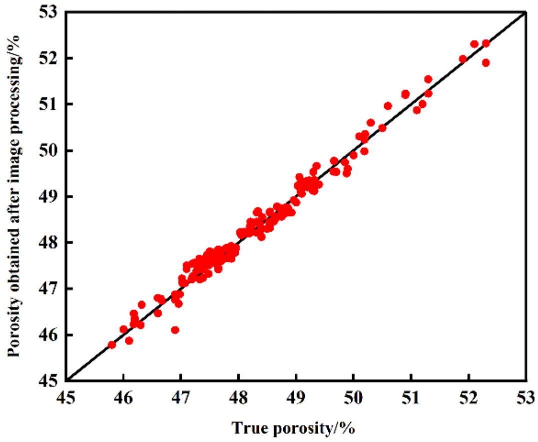

Fig. 4 - Fitting of porosity obtained after image processing to true values

Experimental Procedure

The rice drying experiment was conducted at the Intelligent Agricultural Machinery Equipment Laboratory of Heilongjiang Bayi Agricultural University. To simulate the actual conditions of rice after harvest, the paddy rice underwent moisture adjustment treatment, followed by sealed storage for a period of time and subsequent water spraying. After ensuring the rice absorbed enough moisture, the required rice samples for the experiment were obtained (*Chen et al., 2022*). First, the heat exchanger and fan were activated and allowed to stabilize before loading the rice. The drying process then began, with the dryer completing one cycle every 20 minutes based on real-time operating conditions. During both the early and late stages of the rice drying process, porosity measurements were taken at intervals of 20 minutes and 10 minutes, respectively, and compared with the predicted model. If the fit was satisfactory, the operating efficiency of the heat exchanger and fan was reduced to achieve energy savings. The experiment was then concluded.

Data Preprocessing

To mitigate the impact of differences between feature values on the prediction model, the $mapminmax$ function (*Liang et al., 2019*) was used to normalize the feature data, thereby ensuring the stability of the model's numerical values. The normalization formula is given by Equation 3.

$$y = \frac{(y_{max} - y_{min}) \times (x_{max} - x_{min})}{x_{max} - x_{min}} + y_{min} \tag{3}$$

where:

x_{max} is the maximum value in the original feature data;

x_{min} is the minimum value in the original feature data;

y_{max} is the maximum value after normalization, set to 1;

y_{min} is the minimum value after normalization, set to 0.

Orthogonal Experiment Design

The paddy rice moisture content, paddy rice grain length, and grain bulk height were selected as experimental factors, with paddy rice porosity set as the evaluation criterion. The experiment employed a three-factor, three-level quadratic regression orthogonal rotational combination design to analyze the effects of paddy rice moisture content, paddy rice grain length, and grain bulk height on paddy rice porosity and to construct a regression model. The factor level coding table is shown in Table 1.

Table 1

Encoding of orthogonal experimental factors

Serial Number	Encoding value	Paddy rice moisture content X_1 [%]	Paddy rice grain length X_2 [mm]	Grain bulk height X_3 [mm]
(+1)	+1	23. 41	10. 16	350
(0)	0	18. 93	8. 85	200
(-1)	-1	14. 45	7. 54	50

Development of the Prediction Model

SVR Model

The SVR model is trained using the training set $T= \{(x_1, y_1), \ldots, (x_n, y_n)\}$, they correspond to the input vector and output value of the sample, respectively. During the training process, SVR utilizes a nonlinear mapping $\phi(x)$ to map the training set from a low-dimensional space to a high-dimensional space (*Jin et al., 2024; Yang, 2023; Cui, 2023*). The expression of this process is shown in equation 4. A schematic diagram of the SVR prediction model is shown in Fig. 5.

$$f(x) = \omega\emptyset(x) + b \tag{4}$$

where: ω is the weight; b is the bias.

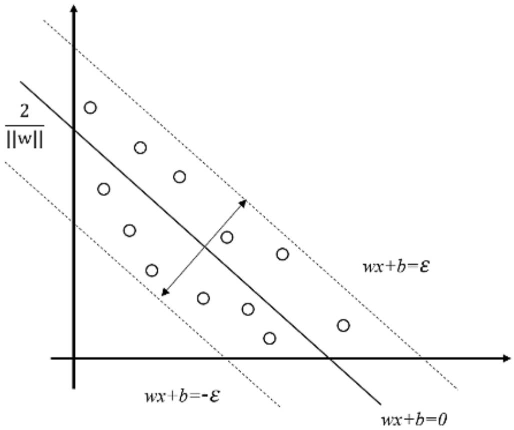

Fig. 5 - SVR prediction schematic diagram

The process of solving the SVR based on the principle of Structural Risk Minimization (SRM) can be represented as solving a constrained optimization problem, as shown in the following equation:

$$\min_{\omega,b}\frac{1}{2}||\omega||^2 + C\sum_{i=1}^{N}(\xi_i^{\Lambda} + \xi_i^{V}) \tag{5}$$

$$s.t. -(k + \xi_i^{V}) \le y_i - (\omega x_i + b) \le k + \xi_i^{\Lambda} \tag{6}$$

$$\xi_i^{\Lambda} \ge 0,\ \ i = 1,2,\cdots,N \tag{7}$$

$$\xi_i^{V} \ge 0,\ \ i = 1,2,\cdots,N \tag{8}$$

where:

C is the penalty parameter, which regulates the complexity of the sample regression model and the fitting accuracy;

ξ_i^{Λ} is the upper-bound slack variable;

ξ_i^{V} is the lower-bound slack variable;

k is the insensitive loss factor.

By introducing the Lagrange multiplier operator and the duality principle, the optimal Lagrange multiplier parameters a^{Λ^*} and a^{V^*} are obtained through the Sequential Minimal Optimization (SMO) algorithm.

By incorporating the kernel function, the nonlinear mapping expression for the SVR is derived as:

$$f(x) = \omega\phi(x) + b = \sum_{i}^{N}(\alpha_i^{\Lambda^*} - \alpha_i^{V^*})K(x_i, x) \tag{9}$$

where: $K(x_i, x) = \phi(x_i)\phi(x)$ is the kernel function.

S0 Algorithm

Snake optimization, as a search strategy, effectively avoids getting trapped in local optima and exhibits a fast convergence rate when approaching the global optimum. The snake algorithm is a global optimization algorithm that simulates the combat and mating behaviors of snakes to achieve optimization. In the combat mode, male snakes compete to obtain the best female mate, while female snakes select the most suitable male for mating (*Su et al., 2022*). The specific process of the snake optimization algorithm is shown in Fig. 6.

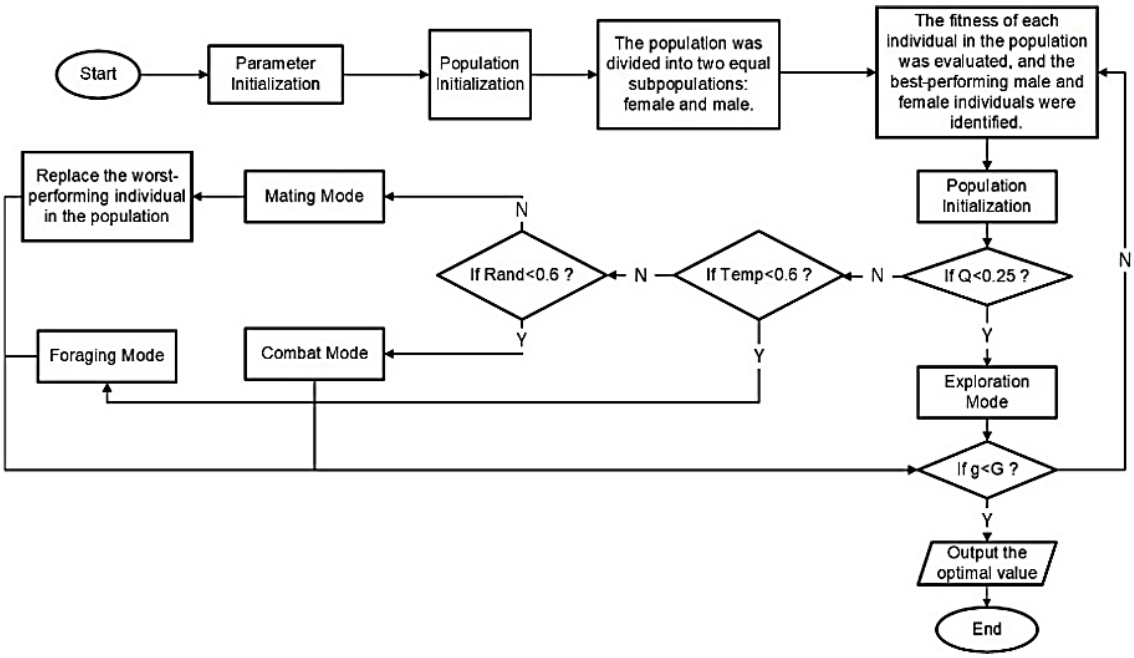

Fig. 6 - Snake algorithm optimization flowchart

Construction of the Paddy Rice Porosity Prediction Model:

The paddy rice moisture content, paddy rice grain length, and grain bulk height, which are three factors affecting porosity, are selected as input variables for the prediction model. The porosity of paddy rice serves as the output variable, and the SO-SVR model is constructed for predicting paddy rice porosity.

In the SVR model, the penalty parameter C and $gamma$ (the parameter of the radial basis function (*RBF*) kernel) are the key parameters influencing its prediction performance. The snake optimization algorithm generates N individuals randomly within the search space as the initial population for computation. The initial population is set to 100, with a maximum iteration count of 50 and a search range between [-1, 1]. The snake population X is divided into male snake group X_m and female snake group X_f. The fitness value of each snake individual is compared with its counterpart, and the individual with the lower fitness value is selected to form a new population.

During the optimization iterations, the parameter values of C and $gamma$ output in each iteration are input into the SVR model. The *Train* function is then called to calculate the fitness, and the output error is used as the fitness function, which is returned to the snake optimization for iterative optimization. This process continues until the fitness function converges.

In each iteration, the SO algorithm produces a new set of C and $gamma$ values. These new parameter combinations are used to train the SVR model, with the prediction error serving as an indicator to assess its performance. Based on the performance evaluation results, the combination of C and $gamma$ that provides the best performance for the SVR model is selected.

Model Accuracy Evaluation Metrics:

The coefficient of determination R^2 and the root mean square error (RMSE) are used to evaluate the accuracy of the neural network model (*Qiu et al., 2023*), as shown in Equations 9 and 10.

$$R^2 = \frac{(n\sum x_i \bullet y_i) - (\sum x_i \bullet \sum y_i)^2}{[n\sum x_i^2 - (\sum xi)^2 \bullet (n\sum y_i^2 - (\sum yi)^2)]} \tag{10}$$

$$RMSE = \sqrt{\frac{1}{n}\sum_{i=1}^{n}(y_i - x_i)^2} \tag{11}$$

where:

n is the number of prediction samples; y_i is the actual value; x_i is the predicted value.

RESULTS

Orthogonal experiment results and analysis

Table 2

Quadratic regression orthogonal rotation combination experiment and results

Number	Paddy rice moisture content X_1 [%]	Paddy rice grain length X_2 [mm]	Grain bulk height X_3 [mm]	Paddy rice porosity Y_1 [%]
1	-1	-1	0	48.37
2	1	-1	0	47.56
3	-1	1	0	48.55
4	1	1	0	47.88
5	-1	0	-1	49.32
6	1	0	-1	48.67
7	-1	0	1	46.91
8	1	0	1	46.18
9	0	-1	-1	49.17
10	0	1	-1	50.19
11	0	-1	1	47.19
12	0	1	1	47.35
13	0	0	0	48.12
14	0	0	0	47.96
15	0	0	0	47.93
16	0	0	0	47.94
17	0	0	0	47.92

The experimental results indicate that under the same conditions, the paddy rice moisture content, paddy rice grain length, and grain bulk height all have an impact on the paddy rice porosity. The analysis of the experimental results is shown in Table 3.

Table 3

Regression coefficient significance and ANOVA for paddy rice porosity model

Parameter	Paddy rice porosity [%]		
	Coefficient	F-value	P-value
Model	14.44	128.55	< 0.0001
X_1	1.02	81.92	< 0.0001
X_2	0.3528	28.27	0.0001
X_3	11.81	946.19	< 0.0001
$X_1 X_2$	0.0049	0.3926	0.5508
$X_1 X_3$	0.0016	0.1282	0.7309
$X_2 X_3$	0.1849	14.81	0.0063
X_1^2	0.3652	29.26	0.0010
X_2^2	0.7095	56.85	0.0001
X_3^2	0.0345	2.76	0.1404
Residual Sum of Squares		0.0874	
Pure Error Sum of Squares		0.0275	
Coefficient of Determination R^2		0.9940	
Adjusted R^2		0.9863	
Predicted R^2		0.9311	
C.V.%		0.2324	

The p-value of the model is less than 0.01, indicating that the regression model for paddy rice porosity is significant and statistically meaningful. The test result for the misfit terms is $p=0.1652$, which is not significant, demonstrating that the regression equation has a good fit and practical relevance. After removing the insignificant factors, the analysis of variance for porosity, shown in Table 3, presents the regression equation for porosity based on the factor coding:

$$Y_1 = 62.27 + 0.43X_1 - 3.97X_2 + 0.001X_3 - 0.001X_2X_3 - 0.01X_1^2 + 0.24X_2^2 \tag{12}$$

Response Surface Analysis

To further visualize and evaluate the influence of various factors on the response variable, Design-Expert 13 software was employed to generate response surface plots. These plots were used to investigate whether the interaction effects among paddy rice moisture content, paddy rice grain length, and grain bulk height lead to significant variations in the porosity of paddy rice.

Fig. 7a illustrates the response surface depicting the interaction between paddy rice moisture content and grain length on paddy rice porosity, under the condition of a grain bulk height of 200 mm. As shown in the figure, porosity increases with grain length, suggesting that longer rice grains result in greater intergranular space within the bulk. In contrast, porosity decreases with increasing moisture content, indicating a negative correlation between moisture content and porosity.

Fig. 7b illustrates the response surface depicting the interaction between paddy rice moisture content and grain bulk height on paddy rice porosity, under the condition of a grain length of 8.85 mm. As shown in the figure, porosity decreases with increasing moisture content, indicating a negative correlation. Similarly, porosity also declines as grain bulk height increases, and the influence of grain bulk height on porosity is observed to be more pronounced than that of moisture content.

Fig. 7c illustrates the response surface depicting the interaction between paddy rice grain length and grain bulk height on paddy rice porosity, under the condition of a moisture content of 18.93%. As shown in the figure, porosity gradually decreases with increasing grain bulk height, when grain length is held constant. Moreover, the influence of grain bulk height on porosity is observed to be more significant than that of grain length.

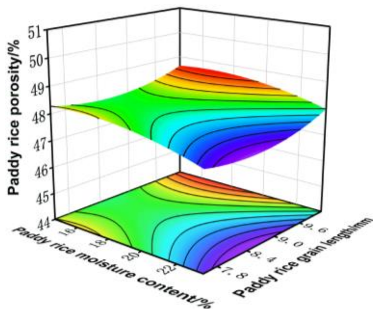

a) The effects of moisture content and grain length on the porosity of paddy rice

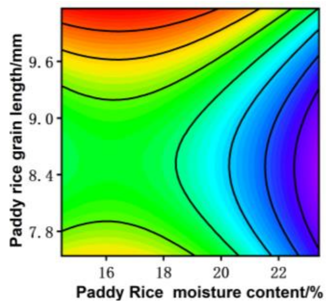

b) Contour plot showing the effects of moisture content and grain length on the porosity paddy rice

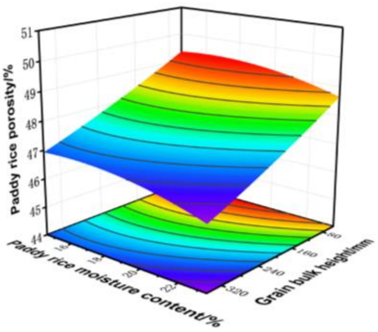

c) The effects of moisture content and grain bulk height on the porosity of paddy rice

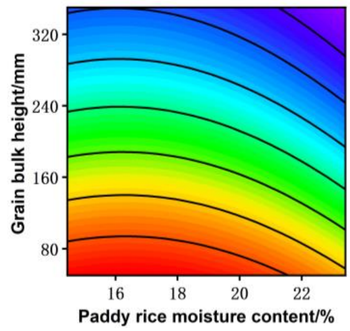

d) Contour plot showing the effects of moisture content and grain bulk height on the porosity of paddy rice

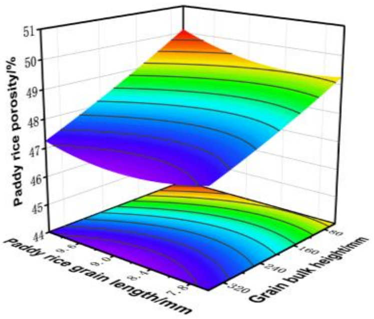

e) The effects of grain length and grain bulk height on the porosity of paddy rice

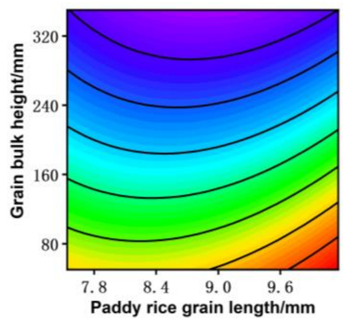

f) Contour plot showing the effects of grain length and grain bulk height on the porosity of paddy rice

Fig. 7 - Effects of moisture content, grain length, and bulk height on paddy rice porosity

Prediction Model Results Analysis

A total of 200 data sets were selected as the sample size, with 80% used for training and 20% for testing. First, the training samples were divided into a training set and a testing set. The input and output samples were then normalized, and the parameters were initialized.

The comparison of rice porosity predicted by the three algorithms for both the training and testing sets is shown in Fig. 8. After training the model, the results were exported to the MATLAB workspace. The simulation results of the three prediction models are presented in Table 4. The R^2 of the SO-SVR algorithm is 0.9913, and the RMSE is 0.0095. Compared to the SVR and BP algorithms, the R^2 increased by 0.0449 and 0.1102, respectively, while the RMSE decreased by 0.0867 and 0.1663.

Table 4

Simulation test results of three algorithms

Type	R^2	RMSE
SO-SVR	0.9913	0.0095
SVR	0.9464	0.0962
BP	0.8811	0.1758

Simulation experiments were conducted for the three prediction models, and the analysis shows that the SO-SVR algorithm demonstrates higher accuracy in predicting rice porosity compared to the SVR and BP algorithms.

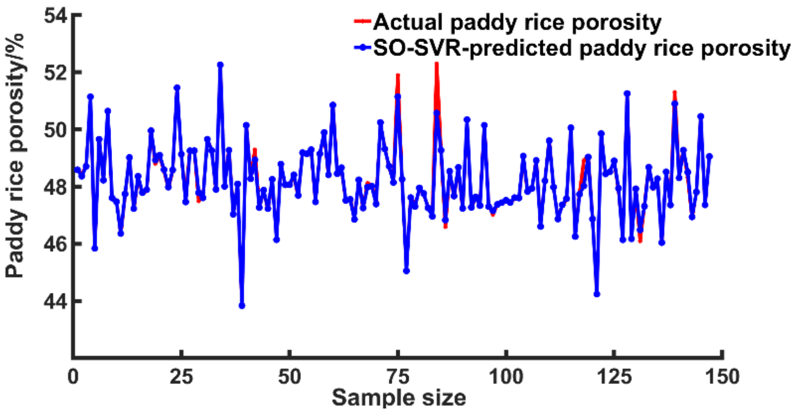

a) SO-SVR algorithm

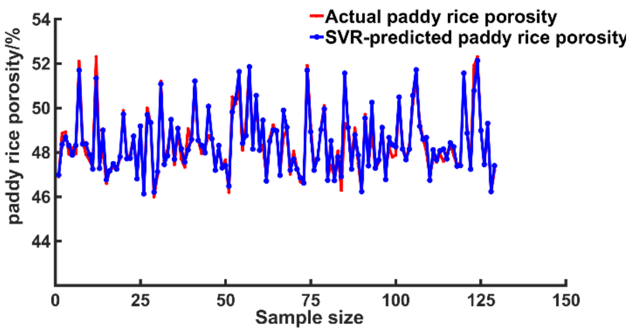

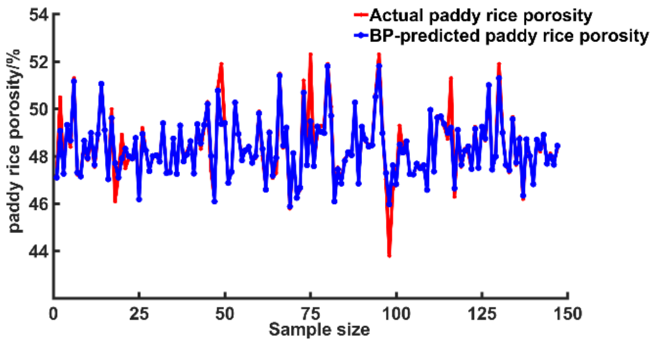

b) SVR algorithm *c) BP algorithm*

Fig. 8 - Comparison between actual paddy rice porosity and predicted values from three algorithms

Model Validation

The rice porosity data collected from the experiment were compared and analyzed against the rice porosity predictions made by the three algorithms. The maximum relative error and average relative error are shown in Table 5.

Table 5

Validation test results of three algorithms

Type	Maximum relative error [%]	Mean Relative Error [%]
SO-SVR	1.95	1.12
SVR	9.23	2.24
BP	14.62	4.36

The SO-SVR algorithm shows a reduction in the maximum relative error by 7.28% compared to SVR and by 12.67% compared to BP. The average relative error is also lower by 3.24% compared to SVR and by 1.12% compared to BP. The error between the rice porosity predicted by the SO-SVR model and the actual rice porosity is smaller, confirming the higher accuracy of the SO-SVR prediction model through experimental validation.

CONCLUSIONS

This study proposes a method for measuring the porosity of paddy rice based on image detection techniques. In the experiment, porosity was determined using an image-based approach, and the results were compared with those obtained from a theoretical method to verify the measurement accuracy. Furthermore, a paddy rice porosity prediction model based on SO-SVR was developed. The SO was used to identify the optimal combination of SVR hyperparameters C and $gamma$, which were then input into the SVR model to minimize prediction error. The optimal values of C and $gamma$ were found to be 4.00 and 3.99, respectively.

Simulation experiments for three rice porosity prediction models were conducted using MATLAB, with a total of 200 data sets selected as the sample size, 80% for training and 20% for testing. The coefficient of determination for SO-SVR was 0.9913, and the root mean square error was 0.0095. The iteration speed and prediction accuracy of the SO-SVR model were superior to those of the SVR and BP algorithms. The results of simulation experiments demonstrate that the SO-SVR-based model provides high accuracy in predicting paddy rice porosity.

Validation experiments were conducted for the three prediction models during the mixed flow drying process. The maximum relative error of the SO-SVR-based prediction model was 1.95%, and the average relative error was 1.12%, both of which were lower than those of the SVR and BP algorithms. The experimental results confirmed the accuracy of the SO-SVR-based rice porosity prediction model during the drying process, showing a good fit with the actual values and a small error. The predictive model proposed in this study enables estimation of paddy rice porosity and rapid assessment of drying degree throughout the drying process. It provides an effective means for monitoring drying performance, reducing energy waste, and optimizing drying operations, thereby improving overall energy efficiency.

ACKNOWLEDGEMENT

This project is supported by the Natural Science Foundation of Heilongjiang Province (LH2022E098).

REFERENCES

[1] Bian, H., Jiang, M. M., Liu, C. S., Yin, J. (2021). Study on the relationship between grain bulk pressure and porosity based on digital image technology (基于数字图像技术的粮堆压力与孔隙率关系研究). *Journal of Henan University of Technology (Natural Science Edition),* Vol.42(02), pp.107-111+120. Henan/China. DOI: 10.16433/j.1673-2383.2021.02.016.

[2] Che, G., Wu, C. S. (2017). Drying Technology and Intelligent Equipment for Typical Agricultural Products (典型农产品干燥技术与智能化装备). *Chemical Industry Press, Beijing, China.*

[3] Chen, Z. F., Che, G., Wan, L. (2022). Numerical simulation and experimental study of paddy rice four-way mixed-flow drying section (稻谷四向通风混流干燥段数值模拟与试验). *Transactions of the Chinese Society of Agricultural Engineering.* Vol.38(24), pp.237-247. Beijing/China.

[4] Chen, X., Cheng, X. D., Long, T. (2019). Study on porosity distribution of wheat bulk in a conical-hopper silo (带锥斗筒仓内小麦堆孔隙率分布研究). *Grain Science and Technology and Economy.* Vol.44(10), pp.48-52. Beijing/China.

[5] Cheon, D. S., Takahashi, M., Kim, T. (2021). Permeability differences based on three-dimensional geometrical information of void spaces. *Journal of Rock Mechanics and Geotechnical Engineering*, 13(2): 368–376.

[6] Cui, F. C., Mao, Z. C., Li, T. T., Li, J. R. (2023). Construction and application of a neural network-based shelf-life prediction model for fresh aquatic products (基于神经网络的生鲜水产品货架期预测模型的构建及应用). *Journal of Chinese Institute of Food Science and Technology.* Vol.23(11), pp.254–265. Beijing/China.

[7] Fujimori, S., Hasegawa, T., Krey, V., A multi-model assessment of food security implications of climate change mitigation[J]. *Nature Sustainability,* 2019, 2(5): 386 396.

[8] Ge, M. M., Chen, G. X., Liu, C. S., Zhang, H. W. (2021). Study on vertical pressure, porosity, and density of different grain types (不同粮种竖向压力孔隙度与密度研究). *Journal of Henan University of Technology (Natural Science Edition).* Vol.42(04), pp.89-95. Henan/China.

[9] Jin, H., Hu, Y. X., Ge, H. J., Hao, Z. P. (2024). Remaining useful life prediction of lithium-ion batteries based on improved GWO–SVR algorithm (基于改进 GWO–SVR 算法的锂电池剩余寿命预测). *Journal of Engineering Science.* Vol.46(03), pp.514–524. Beijing/China.

[10] Khalili, A., Morad, M. R., Matyka, M. (2014). Porosity variation below a fluid-porous interface. *Chemical Engineering Science,* 107: 311-316.

[11] Li, C. Y., Fang, Z. D., Mai, Z. W. (2014). Design and experiment of a porosity measurement device for bulk materials (散体物料孔隙度测定装置设计与试验). *Transactions of the Chinese Society for Agricultural Machinery.* Vol.45(10), pp.200–206. Beijing/China.

[12] Liang, Z. C., Guo, X. W., Song, Y. J., Ma, T. F., Wang, F. (2019). Optimization of polysaccharide extraction from Agaricus bisporus by response surface methodology and its in vitro antioxidant activity (响应面法优化双孢蘑菇多糖提取工艺及其体外抗氧化活性研究). *Journal of Agricultural Science and Technology.* Vol.21(08), pp.161–168. Beijing/China.

[13] Martynenko, A. (2008). The system of correlations between moisture, shrinkage, density, and porosity. *Drying Technology,* 26(12):1497-1500

[14] Moya, M., Aguado, P. J., Ayuga, F. (2013). Mechanical properties of some granular agricultural materials used in silo design. *International Agrophysics,* 27(2): 181-193.

[15] Neethirajan, S., Jayas, D. S., White, N. D. G., Zhang, H. (2008). Investigation of 3D geometry of bulk wheat and pea pores using X-ray computed tomography images. *Computers and Electronics in Agriculture,* 63(2):104–111.

[16] Oliveros, N. O., Hernández, J. A., Sierra-Espinosa, F. Z. (2017). Experimental study of dynamic porosity and its effects on simulation of the coffee beans roasting. *Journal of Food Engineering,* 199: 100-112.

[17] Prasad, S., Gupta, C.P., Behavior of paddy grains under quasi-static compressive loading[J]. *Transactions of the ASAE*, 16(2):328-330

[18] Qiu, J. D., Wang, T. X., Wan, F. X. (2023). Moisture content prediction of shiitake mushroom during vacuum far-infrared radiation drying based on improved BP neural network (基于改进 BP 神经网络的香菇真空远红外辐射干燥含水率预测). *Forestry Machinery & Woodworking Equipment.* Vol. 51(10), pp. 32-38. Beijing/China.

[19] Su, Z.Y. (2022). *Research on intelligent control system for circulating grain dryer (循环式粮食干燥机智能控制系统的研究).* Master's thesis, South China Agricultural University. Guangzhou/China.

[20] Tang, F. Y., Xu, Q., Cheng, X. D. (2017). Study on porosity distribution of paddy rice in silo (筒仓中稻谷的空隙度分布研究). *Journal of the Chinese Cereals and Oils Association.* Vol.32 (12), pp. 110–116. Beijing / China.

[21] Tong, J. J., Li, C. Y., Liu, M. H. (2023). Design and experiment of a porosity detection device for the flowing layer of paddy rice (稻谷流动层孔隙率检测装置设计与试验). *Journal of Chinese Agricultural Mechanization.* Vol. 44(11), pp. 26-31. Beijing/China. DOI: 10.13733/j.jcam.issn.2095-5553.2023.11.005.

[22] Yang, Y., Liu, J. Y., Chen, T. M. (2023). Short-term natural gas load forecasting based on the PSO-SVR model (基于 PSO-SVR 模型的短期天然气负荷预测). *Science Technology and Engineering.* Vol.23(35), pp.15210-15216. Beijing/China.